Competing nematic interactions in a generalized XY model in two and three dimensions

Gabriel A. Canova,* Yan Levin,† and Jeferson J. Arenzon‡
Instituto de Física, Universidade Federal do Rio Grande do Sul, CP 15051, 91501-970 Porto Alegre RS, Brazil
(Received 29 June 2016; published 30 September 2016)

We study a generalization of the XY model with an additional nematic-like term through extensive numerical simulations and finite-size techniques, both in two and three dimensions. While the original model favors local alignment, the extra term induces angles of $2\pi/q$ between neighboring spins. We focus here on the $q = 8$ case (while presenting new results for other values of q as well) whose phase diagram is much richer than the well-known $q = 2$ case. In particular, the model presents not only continuous, standard transitions between Berezinskii-Kosterlitz-Thouless (BKT) phases as in $q = 2$, but also infinite-order transitions involving intermediate, competition-driven phases absent for $q = 2$ and 3. Besides presenting multiple transitions, our results show that having vortices decoupling at a transition is not a sufficient condition for it to be of BKT type.

DOI: 10.1103/PhysRevE.94.032140

I. INTRODUCTION

Two-dimensional (2D) models with U(1) group symmetry and isotropic, short-range interactions do not present a standard second-order transition as a consequence of the Mermin-Wagner theorem [1]. Indeed, fluctuations (Goldstone modes) destroy any long-range order, even at low temperatures. Nonetheless, 2D models such as the XY do present two different phases, separated by an infinite-order phase transition at $T_{\rm KT}$ known as the Berezinskii-Kosterlitz-Thouless (BKT) transition [2–4]. The low-temperature phase is characterized by bound pairs of vortices and antivortices and power-law decaying correlations driven by the spin waves, while above the critical temperature the vortices decouple and correlations decay exponentially. Moreover, unlike the usual thermodynamic phases, the low-temperature, quasi-long-range order BKT phase is critical at all temperatures below $T_{\rm KT}$. At this temperature, the helicity modulus, which is the order parameter that measures how the system responds to a global twist [5–7], has a universal, discontinuous jump signaling the decoupling of vortices and antivortices.

Here we study a generalization of the XY model with a competing term that favors a different alignment angle, depending on the parameter q, $\mathcal{H} = \sum_{\langle ij\rangle} U(\theta_i - \theta_j)$, where

$$U(\phi) = -\Delta\cos\phi - (1-\Delta)\cos(q\phi), \qquad (1)$$

with $0 \leqslant \Delta \leqslant 1$. The sum is over nearest neighbors, $0 \leqslant \theta_i < 2\pi$, and the usual XY model, with ferromagnetic interactions is recovered either when $\Delta = 1$ or $q = 1$. For $\Delta = 0$ the pure nematic term induces skewed alignments with angles $2k\pi/q$, where $k \leqslant q$ is an integer. Since the partition function for the cases $\Delta = 0$ and 1 can be mapped onto each other by the transformation $q\theta_i \to \bar{\theta}_i$, the critical temperature [8] is the same, $T_{\rm KT}(\Delta = 0) = T_{\rm KT}(\Delta = 1) \simeq 0.893$. This transition, from the high-temperature paramagnetic phase to a phase where there is local, non-long-ranged ordering, either nematic (for small Δ) or ferromagnetic (large Δ), is a BKT transition. In the intermediate region where both terms compete, although new phases may appear at low temperature, the transition from the paramagnetic phase seems to be BKT for all values of Δ (albeit it remains possible that a non BKT transition may exist close to the multicritic point [9,10]). Interestingly, since the presence of a competing term helps to disrupt both the nematic and ferromagnetic orderings, the transition temperature $T_{\rm KT}(\Delta)$ is smaller at intermediate values of Δ. At its minimum, that gets closer to $\Delta = 0.5$ as q increases, several transition lines meet at a multicritical point, $\Delta_{\rm mult}$. The parameter Δ can tune the relative strength of the two terms in Eq. (1) and, as a consequence, which type of vortices, integer or semi-integer (see below) is going to be relatively suppressed. This class of models, with ferromagnetic and/or antiferromagnetic interactions, was used to model the interlayer interactions of stacked bent-core molecules in liquid crystals [11], DNA packing [12], structural phases of cyanide polymers [13,14], quasicondensation in atom-molecule, bosonic mixtures [15–17], and out-of-equilibrium self-propelled polar particles [18], with a similar, albeit dynamical, phase diagram in the latter case.

For $q = 2$, in 2D, there are two transitions for $\Delta < \Delta_{\rm mult}$ [9,10,19–26]: as T decreases there is first a BKT transition to a phase with a local nematic ordering and, at a lower temperature, a symmetry breaking transition in the Ising universality class to a phase with a local ferromagnetic alignment. In spite of the presence of a standard, continuous transition, both phases are critical at every temperature, but differ by the nature of the coupled topological defects they contain (see below). On the other hand, for $\Delta > \Delta_{\rm mult}$, there is a single BKT transition from the paramagnetic phase. A similar phase diagram was obtained in 3D [27], but while the transition from the nematic to the ferromagnetic phase is still Ising like (3D), the transition to the paramagnetic phase, for all Δ, is continuous with exponents belonging to the 3DXY universality class (under different conditions, a BKT transition in 3D may occur as well [28–31]). A closely related class of models consists on a double XY model with an extra term coupling the two variables that in the limit of strong coupling recovers the Hamiltonian Eq. (1) [17,32,33]. The models with $q > 2$ have been recently investigated as well [34,35] (higher harmonics have been also considered in Ref. [36] in a related albeit different model). The overall phase diagram is similar for both $q = 2$ and 3, the main difference being that for $q = 3$ the transition between the ferromagnetic-like ($\mathbf{F}_0$) and the nematic-like ($\mathbf{N}$) phase is in the three-states Potts universality class (for all q, the

*gabriel.canova@ufrgs.br
†levin@if.ufrgs.br
‡arenzon@if.ufrgs.br

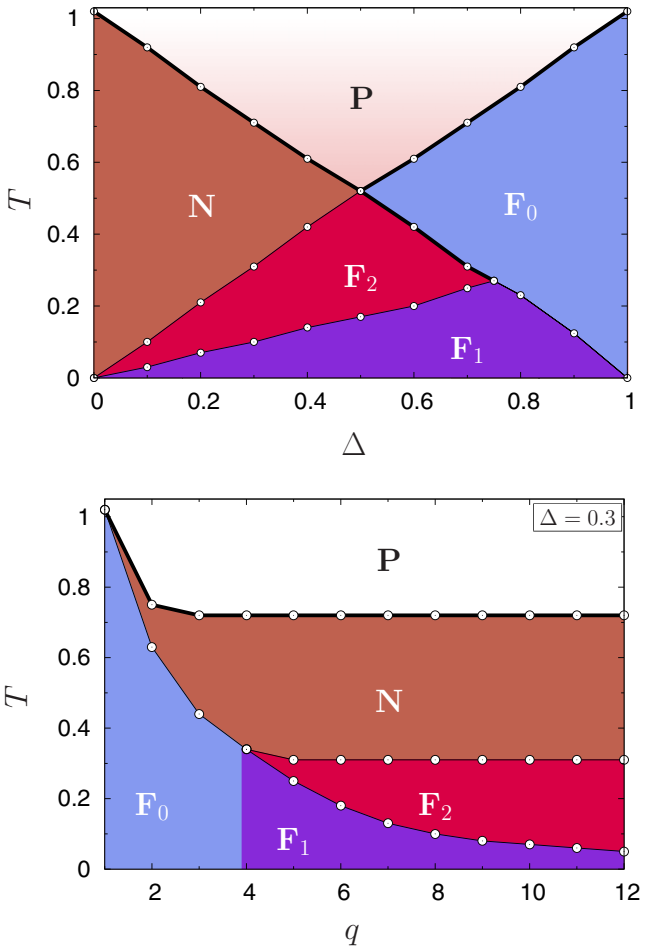

FIG. 1. (Top panel) Qualitative phase diagram for the 2D generalized XY model with $q = 8$. The points correspond to the maxima of the specific heat for $L = 64$ while the lines (thick and thin for BKT and second-order transitions, respectively) are just a guide to the eyes. (Bottom panel) Transition lines for several values of q for $\Delta = 0.3$. There is a bifurcation of the **N**-$\mathbf{F}_0$ transition for $q > 4$, similar to what happens in the Clock model with $\mathbb{Z}_q$ symmetry. The lowest transition line decreases as q^{-2}.

N phase is unstable at low enough temperature if $\Delta \neq 0$). Moreover, for all values of Δ, the temperature at which the BKT transition occurs obeys [35] the lower bounds obtained by Romano [37]. A related coupled XY model has been studied, based on Ref. [38], for $q = 3$ both in 2D [32,39] and 3D [40] and for $q = 6$ on a triangular lattice [41].

For $q = 8$ [34], a representative large value of q, several new features are present as the former pseudoferromagnetic phase seems to split into several regions with different quasi-long-range ferromagnetic orderings, $\mathbf{F}_0$, $\mathbf{F}_1$, and $\mathbf{F}_2$ (some hints of an extra phase appear in an earlier study [41] of coupled XY models with a onsite coupling inducing a $q = 6$ order); see Fig. 1. Simulations with small lattice sizes [34] were consistent with the $\mathbf{F}_1$-$\mathbf{F}_0$ and $\mathbf{F}_2$-$\mathbf{F}_0$ transitions being in the BKT universality class. Interestingly, for some values of Δ, there are two BKT transitions as the temperature is lowered. The results of Ref. [34] for $q = 8$ were preliminary and some were not conclusive. Indeed, the lattice sizes used were too small to confirm the 2D Ising universality class of the transition $\mathbf{F}_1$-$\mathbf{F}_2$ and the evidence for the existence of the transition $\mathbf{F}_1$-$\mathbf{F}_0$ was admittedly quite weak. Therefore, this work is aimed not only to solve these issues, providing further data supporting or clarifying the previous existence and universality claims, but also to extend to 3D the results for both $q = 3$ and 8. In addition, other interesting questions remain open. How, as q increases, the phase diagram changes from two to four (locally) ordered phases? The nematic term, albeit with continuous variables, has some similarity with the discrete Clock model. How similar is the behavior of both models? In order to answer these questions, we present new results for larger lattices (on the square and cubic lattices with periodic boundary conditions) also exploiting the power provided by GPU computation and cluster algorithms (Wolff [42] for small system sizes and Swendsen-Wang for the large ones [43]). The cluster algorithms were from Ref. [44] and the random number generator, a linear feedback shift register based on the XOR operator, from Ref. [45]. A large number of samples were used on the averages and usually the errors were smaller than the symbols used in the figures (with the exception of a few noisy quantities, e.g., Figs. 4 and 16).

In order to clarify the nature of the phase transitions, we consider the modulus of the generalized magnetization,

$$m_k = \frac{1}{N}\left|\sum_i \exp(ik\theta_i)\right|, \tag{2}$$

and the corresponding susceptibilities and Binder cumulants [46,47],

$$\chi_k = \beta N\left(\langle m_k^2\rangle - \langle m_k\rangle^2\right), \tag{3}$$

$$U_k = \frac{\langle m_k^2\rangle^2}{\langle m_k^4\rangle}, \tag{4}$$

where $1 \leqslant k \leqslant q$, $N = L^d$, and $\langle \ldots \rangle$ means thermal average. The specific heat is also measured in order to obtain a rough location of the transition lines on the phase diagram. In 3D, because the low-temperature phase has genuine long-range order, or for second-order transitions that are present in 2D, the critical exponents β, γ, and ν may be obtained via standard finite-size scaling relations, $m = L^{-\beta/\nu} f(tL^{1/\nu})$ and $\chi = L^{\gamma/\nu} g(tL^{1/\nu})$ with $t \equiv T/T_c - 1$. In 2D, however, because the pseudo-ordered phase is critical everywhere, the magnetization goes to zero while the susceptibility diverges in the thermodynamic limit for all temperatures below the BKT transition.

For a BKT transition, the proper order parameter is the helicity modulus [5,6,48], the response of the system upon a small overall twist τ of spins in a particular direction. It is defined as $\langle \Upsilon \rangle \equiv \partial^2 F/\partial \tau^2|_{\tau=0} = \langle e \rangle - N\beta\langle s^2\rangle$, where F is the free energy, $e \equiv N^{-1}\sum_{\langle ij\rangle_x} U''_{ij}(\phi)$ and $s \equiv N^{-1}\sum_{\langle ij\rangle_x} U'_{ij}(\phi)$ (the sum is over the nearest neighbors along the direction of the twist), $\phi = \theta_i - \theta_j$, and $U_{ij}(\phi)$ is the potential between spins i and j. Following Ref. [10], for the Hamiltonian Eq. (1),

$$\Upsilon = \frac{1}{N}\sum_{\langle ij\rangle_x}[\Delta\cos\phi + q^2(1-\Delta)\cos(q\phi)] - \frac{\beta}{N}\left\{\sum_{\langle ij\rangle_x}[\Delta\sin\phi + q(1-\Delta)\sin(q\phi)]\right\}^2. \tag{5}$$

To improve the accuracy, we average Υ both along the horizontal and vertical directions. Moreover, a fourth-order helicity modulus Υ_4 can be introduced in a similar way [48], $\langle\Upsilon_4\rangle \equiv \partial^4 F/\partial\tau^4|_{\tau=0}$, with the perturbed free energy, up to fourth order, given by $F(\tau) \simeq \langle\Upsilon\rangle\tau^2/2! + \langle\Upsilon_4\rangle\tau^4/4!$. The BKT theory predicts, for the original XY model, that the helicity modulus is zero within the disordered phase and jumps to a finite value at the transition to the ordered phase, where the critical temperature is given by the condition $\Upsilon(T_{\rm KT}) = 2T_{\rm KT}/\pi$ [5,6]. This transition is driven by the decoupling of pairs of integer vortices and antivortices. Since the critical temperature must be the same for both $\Delta = 0$ and 1, the condition becomes $\Upsilon(T_{\rm KT}) = 2T_{\rm KT}/\lambda^2\pi$, where $\lambda = 1/q$ is the charge of the vortex. The q^2 factor is introduced because Eq. (5), for $\Delta = 0$ and 1, differs by this factor. For $q = 2$, the topological excitations in the nematic phase (small Δ) are the *half*-vortices, with related charge $\lambda = \pm 1/2$ [10,20,22,24]. For $q = 3$, vortices excitations were recently found, related to a $\lambda = \pm 1/3$ charge [34,35] in the nematic phase. For larger q, however, since several new phases may be present (see below), it remains unclear what kind of topological excitation each phase does have and which is the nature of each transition. It is possible to somewhat characterize the vortices through the winding number, obtained by summing the phase difference $\phi = \theta_i - \theta_j$ counterclockwise around every site, including all nearest neighbors and taking care that $|\phi| \leqslant \pi$ [49]. For an integer vortex, this sum is $\pm 2\pi n$ and the density of vortices is $\rho_{\rm v} \equiv N_{\rm v}/N$, where $N_{\rm v}$ is the total number of vortices (that may also be distinguished by their sign). This is also easily generalized to semi-integer vortices.

The paper is organized as follows. In Sec. II A we present an improved analysis of the $q = 8$ case in 2D with larger lattices and additional observables [34] sometimes presenting, for the sake of comparison, results for other values of q as well. Then, Sec. II B shows the results for both $q = 3$ and 8 in 3D. In Sec. III we discuss these results and present our conclusions.

II. RESULTS

A. 2D

The phase diagram has the same topology for both $q = 2$ [10,20,22,24] and 3 [34,35]. Besides the paramagnetic phase (**P**) at high temperatures, there are two phases with quasi-long-range order, each one associated with the pure cases at $\Delta = 0$ and 1. The former is a nematic-like phase (**N**) while the latter has local ferromagnetic ordering ($\mathbf{F}_0$). The **N**-$\mathbf{F}_0$ transition is second order and is either in the Ising or in the three states Potts model universality class for $q = 2$ and 3, respectively. Reference [34] also considered the $q = 8$ case in which the region previously occupied by $\mathbf{F}_0$ separates in three phases, all having local ordering similar to the ferromagnetic state (to be discussed in detail below). Through the position of the specific heat peak, we obtain a rough estimate of the phase boundaries for several values of q (not being very precise, the transition line is somewhat displaced). For $q = 2$ and 3 the **N**-**P** BKT transition runs very close to the $T_{\rm KT}(0)(1 - \Delta)$ line, the lower bound for the critical temperature predicted in Ref. [37], and ends at the multicritical point ($\Delta_{\rm mult}$) where several transition lines meet. In these two cases, on the other hand, since the multicritical point is still far from $\Delta = 0.5$, the $\mathbf{F}_0$-**P** BKT transition obeys, but is not so close to the corresponding lower bound, $T_{\rm KT}(\Delta) \geqslant T_{\rm KT}(0)\Delta$, for $\Delta \geqslant \Delta_{\rm mult}$. An important, yet open, issue is how this complex structure unfolds as q increases. As q increases, $\Delta_{\rm mult}$ approaches 0.5 and both BKT transitions to the **P** phase roughly follow those lower bounds (see, e.g., the thick border of phase **P** in Fig. 1). A new transition line appears for $q = 4$, extending from the multicritical point down to the corner at $\Delta = 1$ and $T = 0$, dividing the $\mathbf{F}_0$ phase in two, with a new phase, $\mathbf{F}_1$, being created below both **N** and $\mathbf{F}_0$ for all $0 < \Delta < 1$. For $q = 5$, the **N**-$\mathbf{F}_1$ transition splits in two, creating another intermediate phase, $\mathbf{F}_2$: there is local alignment along several directions, as in the **N** phase, all of them belonging to the same half-plane, as in the $\mathbf{F}_1$ phase. Along with that, the multicritical point also bifurcates, originating a new point where all the $\mathbf{F}_i$ phases meet. Differently from the **N** and $\mathbf{F}_0$ phases that are driven, respectively, by the pure first and second terms in Eq. (1), the new phases, $\mathbf{F}_1$ and $\mathbf{F}_2$, are driven by the competition between these two terms and, as will be seen below, have a mixture of the topological defects that characterize both **N** and $\mathbf{F}_0$. The region occupied by the new phase, $\mathbf{F}_2$, increases with q and the critical temperature at the $\mathbf{F}_1$-$\mathbf{F}_2$ border decreases as q^{-2}. These scenarios are summarized in the bottom panel of Fig. 1 for $\Delta < \Delta_{\rm mult}$ and we remark the resemblance with Fig. 1 from Ref. [50] for the Clock model, whose symmetry is discrete. Indeed, a similar sequence of phase splitting transitions occurs in that model [51,52]. The two transitions, from the para to the ferromagnetic phase in the Clock model and **N**-$\mathbf{F}_2$ here, are in the Ising universality class for $q = 2$ and 4, but belong to the three states Potts model for $q = 3$. Moreover, while here a new phase ($\mathbf{F}_2$) appears for $q > 4$, in the Clock model, a similar, intermediate phase with coarse grained U(1) symmetry (and BKT nature) appears as well, between the paramagnetic and the low temperature, ferromagnetic phase. In both models, the transition temperature to the lowest temperature phase decreases as q^{-2} and, as $q \to \infty$, this phase shrinks and disappears. By suppressing $\mathbf{F}_1$ in this limit, only four phases remain in the phase diagram once again. For $q > 5$, remarkably, while in the Clock model, whose spins are discrete, the two transitions are BKT, here, at least for those values of q that we studied, the transitions from $\mathbf{F}_2$ to both **N** and $\mathbf{F}_1$ seems to be of second order. We now describe in detail the nature of the phases and transitions for $q = 8$.

Figure 2 shows the behavior of the helicity modulus $\langle\Upsilon\rangle$ for three vertical cuts of the phase diagram. In the thermodynamical limit, a BKT transition is signaled by a discontinuous jump of the helicity from $\Upsilon(T_{\rm KT}) = 2T_{\rm KT}/\lambda^2\pi$ to 0. For a finite system, it is expected [53] that the critical temperature reaches logarithmically its asymptotic value as the system size increases,

$$\Upsilon_{\rm fit}(L) = \frac{2TA}{\pi}\left(1 + \frac{1}{2}\frac{1}{\log CL}\right), \tag{6}$$

where A and C are fitting parameters. Notice that in order to present such a behavior, the curves must be size dependent close to the transition. The parameter A, the vorticity, provides an estimate to $1/\lambda$ at the transition [10]. Applying Eq. (6), when appropriate, and minimizing the quadratic error as defined in Refs. [10,35], we find either $A \simeq 64$ or 1, depending on

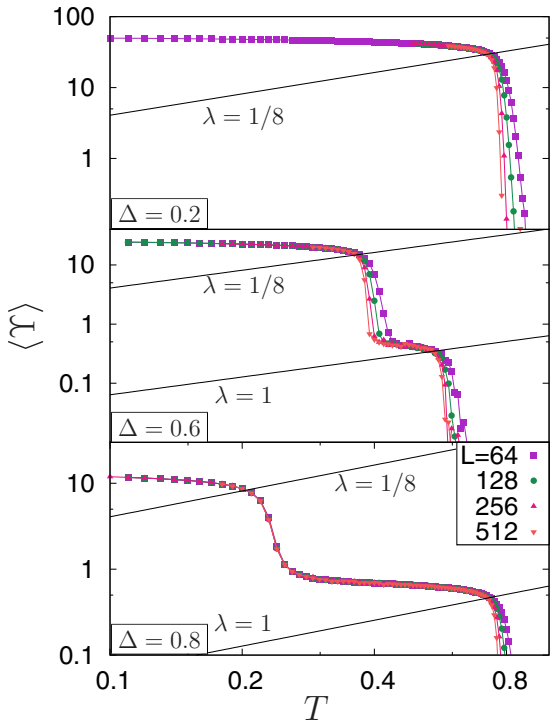

FIG. 2. Helicity modulus vs. temperature, in log-log scale, for the 2D, $q = 8$ model with $\Delta = 0.2$ (top panel), 0.6 (middle panel), and 0.8 (bottom panel). The crossing points of $\langle\Upsilon\rangle$ with the straight lines $2T/\lambda^2\pi$ with $\lambda = 1$ or $1/8$ mark the putative transitions. For $\Delta = 0.2$, at the **N**-**P** transition, $\lambda = 1/8$. For $\Delta = 0.6$ there are two BKT transitions with increasing temperatures, $\mathbf{F}_2$-$\mathbf{F}_0$ and $\mathbf{F}_0$-**P**, with $\lambda = 1/8$ and 1, respectively. Both jumps are size dependent while $\langle\Upsilon\rangle$ has no jump at the transition $\mathbf{F}_1$-$\mathbf{F}_2$ occurring at a lower temperature. When $\Delta = 0.8$, only for the $\mathbf{F}_0$-**P** transition there is an observable size dependence of $\langle\Upsilon\rangle$. At $T \simeq 0.2$, there is a large but smooth change without any perceptible size dependence (within the range considered here). In all cases, the helicity vanishes at the transition to the high-temperature phase.

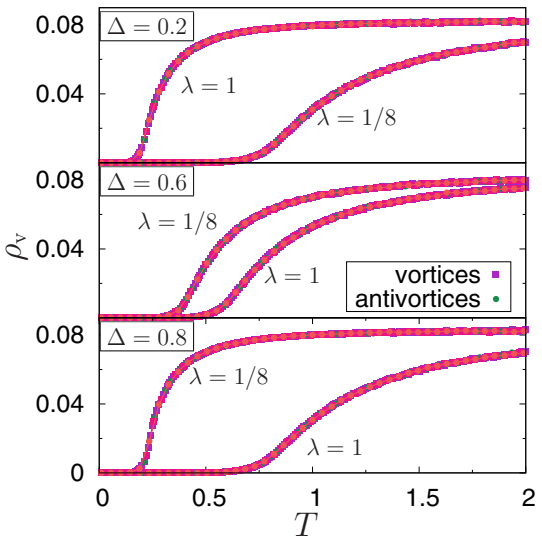

FIG. 3. Density of vortices and antivortices vs. temperature for the 2D, $q = 8$ model for several values of Δ. The behavior is size ($L = 64$ and 256) and vorticity (positive or negative) independent since all sets collapse onto each other. As $T \to \infty$, all curves approach the asymptotic value 1/12 [54] as T^{-2}.

the transition, corresponding to a $\lambda \simeq 1/8$ (fractional) or 1 (integer) charge, respectively. Figure 3 shows the density ρ_v of vortices and antivortices for the same three values of Δ of Fig. 2. There seems to be no size dependence as the curves for both $L = 64$ and 256 perfectly match. No distinction exists also between the number of vortices and antivortices: whether free or bound, their densities are always the same. Vortices unbind close to all transitions shown in the phase diagram, as shown by an increase in the density of vortices, except for the $\mathbf{F}_1$-$\mathbf{F}_2$ one. Thus, both species of vortices, integer and fractional, remain bounded inside $\mathbf{F}_1$ and $\mathbf{F}_2$ and when transitioning to either the **N** or $\mathbf{F}_0$ phases one of the species unbinds, while only at the border with the **P** phase occurs the unbinding of the remaining vortices (where the helicity becomes zero). In all cases, ρ_v monotonously increases, attaining a limiting value when $T \to \infty$ [54]. However, in this limit, because of the strong thermal noise, no vortex exists, and the finite result is an artifact of the lattice discretization that uses a small number of sites around each site in the definition of ρ_v. This is similar to the geometric clusters, group of nearest neighbors parallel spins, whose size distribution at $T \to \infty$ is an exponential, but the physical, Coniglio-Klein clusters of correlated spins correspond to single sites. Indeed, with the above definition of ρ_v, the probability of obtaining a (unitary winding number) vortex purely by chance is (the same result applies for antivortices as well)

$$P_4 = \frac{1}{(2\pi)^3}\int_0^{\pi} d\theta_2 \int_{\theta_2}^{\theta_2+\pi} d\theta_3 \int_{\max(\pi,\theta_3)}^{\min(2\pi,\theta_3+\pi)} d\theta_4 = \frac{1}{12},$$

where the angle θ_i is the state of each neighbor spin (and $\theta_1 = 0$). This asymptotic value is approached as $|\rho_v - 1/12| \sim T^{-2}$ when $T \to \infty$ (although the coefficients differ for integer and semi-integer vortices). In an attempt to get closer to the continuous case, we may generalize the definition and consider loops with n sites around each spin. While for small n this can be done analytically, as n increases one has to resort to numerical evaluations. Combining these results, we conjecture that P_n is given by

$$P_n = \frac{1}{(n-1)!}\left(1 - \frac{n}{2^{n-1}}\right).$$

This expression decreases very fast as n increases, since it become exponentially more difficult to have a vortex by chance alone. This refined classification gives indeed a peaked density of vortices close to the transition but does not change the point at which the vortices unbind. For all $\Delta < \Delta_{\text{mult}}$ (top panel on Figs. 2 and 3) there is an **N**-**P** transition with a discontinuous jump of the helicity (notice the size dependence that indicates a BKT transition) accompanied by the unbinding of the fractional charges, Fig. 3. Once in the paramagnetic phase, the full U(1) symmetry is recovered, vortices and antivortices are no longer bound together, and the helicity vanishes. Although not visible on the scale of Fig. 2 (top panel), there is a tiny, size-independent decrease of the helicity when the border $\mathbf{F}_2$-**N** is crossed as well, indicating a non-BKT transition. Nonetheless, the integer vortices decouple at this transition

(Fig. 3). Inside the phases $\mathbf{F}_1$ and $\mathbf{F}_2$, both kinds of vortices are present and remain bound in vortex-antivortex pairs. For $\Delta > \Delta_{\rm mult}$, the transition $\mathbf{F}_0$-$\mathbf{P}$ involves the dissociation of the integer charges, $\lambda \simeq 1$ (lower straight line in middle and bottom panels of Figs. 2 and 3). In this case, the fractional charges decouple at a lower temperature as can be seen in Fig. 3. The $\Delta = 0.6$ case (middle panel) is an example with two consecutive discontinuous decreases of the helicity, both associated with unbinding of vortices and BKT transitions [34] (notice the size dependence). At the first, lower T transition ($\mathbf{F}_2$-$\mathbf{F}_0$), only the fractional vortices decouple and the helicity decreases to a smaller value corresponding to the integer vortices. Notice that because of the q^2 factor in the definition of $\langle\Upsilon\rangle$, the contribution from fractional vortices is significantly higher than the one from the integer vortices. There is a similar decrease in the bottom panel, without the size dependence characteristic of the BKT transition, which hints to a non-BKT nature of the transition $\mathbf{F}_1$-$\mathbf{F}_0$. While the $\mathbf{N}$ and $\mathbf{F}_0$ phases have either fractional or integer bound vortices, respectively, the phases $\mathbf{F}_1$ and $\mathbf{F}_2$, driven by the competition between the two terms in the potential, have mixed charges, with both species of vortices coexisting and bound in vortex-antivortex pairs. It is indeed because of this coexistence inside both phases $\mathbf{F}_1$ and $\mathbf{F}_2$, with no unbinding whatsoever at the transition, that the helicity does not show any particular feature as the border $\mathbf{F}_1$-$\mathbf{F}_2$ is crossed. Summarizing the evidence gathered from the helicity and the density of vortices, besides the two transitions to the paramagnetic phase, also the $\mathbf{F}_2$-$\mathbf{F}_0$ transition is BKT (all shown as thick lines in the phase diagrams of Fig. 1). Further evidence (not shown) is provided by the susceptibility, Eq. (3), whose behavior is consistent with the one expected at a BKT transition: despite the absence of long range order, finite systems still have a finite magnetization and a divergent susceptibility that scales, for finite systems, as $\chi(T_{\rm KT}) \sim L^{2-\eta}$, with $\eta = 1/4$ at the BKT transition and nonuniversal values inside the low-temperature phase. Similar information is conveyed in Fig. 4, for $\Delta = 0.8$, by the fourth-order helicity modulus, $\langle L^2\Upsilon_4\rangle$, that is expected to diverge at a

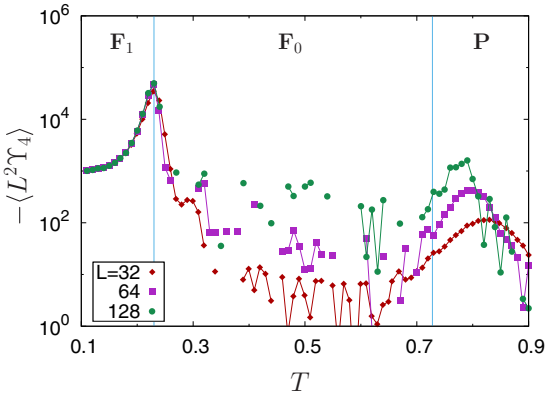

FIG. 4. High-order helicity for the 2D, $q = 8$ case with $\Delta = 0.8$ at the $\mathbf{F}_1$-$\mathbf{F}_0$ (left) and $\mathbf{F}_0$-$\mathbf{P}$ (right) transitions. In the intermediate $\mathbf{F}_0$ phase the results are noisier while both at the paramagnetic and $\mathbf{F}_1$ phases these fluctuations are much suppressed either by the smaller correlation between spins or the larger stiffness of the system, respectively.

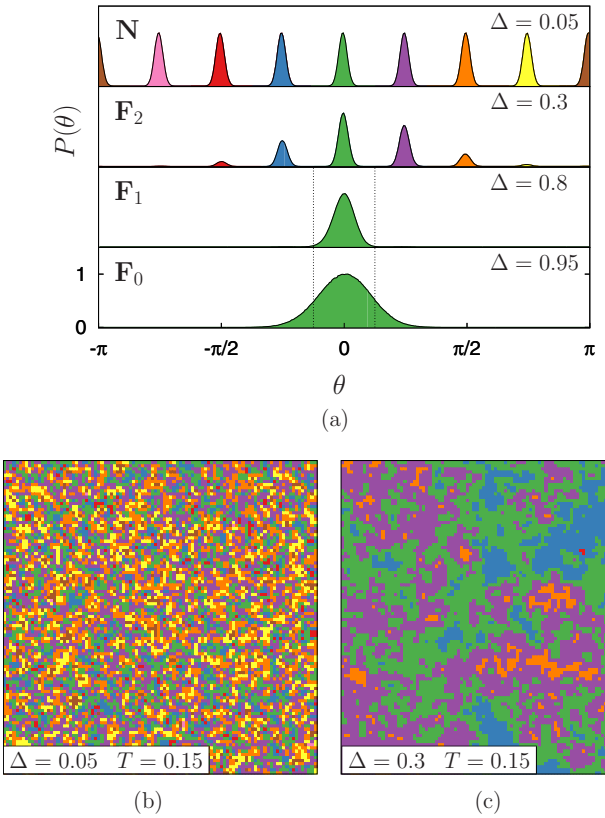

FIG. 5. (a) Distribution of orientations in a single configuration with $L = 1024$ and several values of Δ taken from a horizontal cut of the phase diagram at $T = 0.15$, corresponding to the several low-temperature phases. The vertical dotted lines show that at the $\mathbf{F}_1$-$\mathbf{F}_0$ transition, the width of the distribution becomes larger than $1/8$ of the circle. Snapshots of a 100^2 region of typical configurations in the $\mathbf{N}$ (b) and $\mathbf{F}_2$ (c) phases. The color indicates to which peak of the corresponding panel in (a) the spin belongs to.

BKT transition [48]. We can see that the fourth-order helicity increases only at the transition $\mathbf{F}_0$-$\mathbf{P}$ while at the $\mathbf{F}_1$-$\mathbf{F}_0$ there is no apparent size dependence, again signaling the different nature of both transitions.

Having shown evidences that the transitions $\mathbf{F}_2$-$\mathbf{N}$, $\mathbf{F}_1$-$\mathbf{F}_2$, and $\mathbf{F}_1$-$\mathbf{F}_0$ are not BKT, we now describe the properties of these lines, in particular to which universality classes they belong to. Figure 5(a) shows, for a single configuration, the distribution of the spins [34]. As shown in Ref. [34], the transition between $\mathbf{F}_2$ and $\mathbf{N}$ corresponds to a reflection symmetry breaking transition in the Ising universality class where, from the eight preferential directions symmetrically disposed around the circle in the $\mathbf{N}$ phase, only four remain, all in the same half-plane, after the transition. This is shown in the top two panels while typical configurations for these two phases, in which each peak of the distribution was colored differently are shown in Figs. 5(b) and 5(c). We notice in Fig. 5(b) that the ferromagnetic interaction, being small for $\Delta = 0.05$, does not build clusters with spins belonging to the same peak, instead, neighboring spins tend to obbey the nematic term. For a larger Δ, Fig. 5(c), even if the temperature is slightly higher, the ferromagnetic term increases the size of the clusters (notice also that the system is magnetized in this case). Since

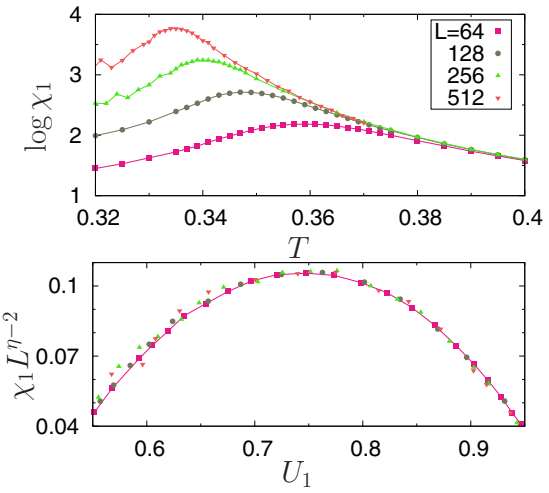

FIG. 6. The transition $\mathbf{F}_2$-$\mathbf{N}$ in the 2D case for $q=8$ and $\Delta=0.35$. The susceptibility χ_1 (top panel) as a function of temperature close to the transition at $T_c \simeq 0.325$. (Bottom panel) Rescaled susceptibility vs. the Binder cumulant for several system sizes. The data collapse is obtained with the Ising 2D exponent $\eta = 1/4$. All logarithms in this work are base 10.

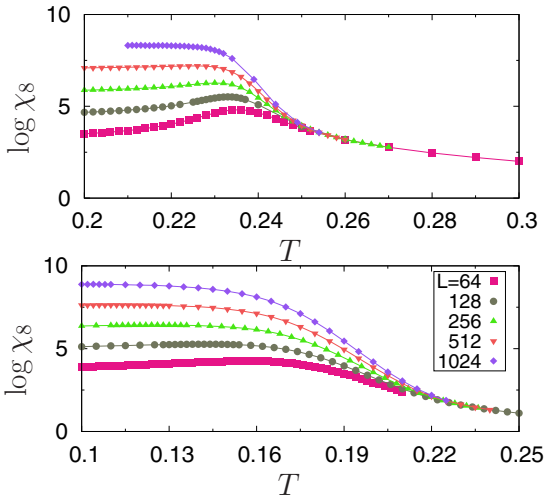

FIG. 7. Susceptibility vs. temperature for the 2DXY model with $q = 8$ at the $\mathbf{F}_1$-$\mathbf{F}_0$ transition for $\Delta = 0.8$ (top) and 0.9 (bottom). At the transition points (notice that due to the logarithmic scale, the maximum of each curve is not clearly seen in the figure), the susceptibility scales as $\chi_8^*(\Delta = 0.8) \sim L^{1.43(5)}$ and $\chi_8^*(\Delta = 0.9) \sim L^{1.74(2)}$.

in phase $\mathbf{F}_2$ spins have a preferred direction, finite systems are magnetized, $m_1 > 0$, and its associated susceptibility, χ_1, presents a divergence as the temperature decreases towards the transition. Figure 6, top panel, shows χ_1 as a function of the temperature for several system sizes for $\Delta = 0.35$. At the critical temperature, $\chi_1 \sim L^{1.752(1)}$, consistent with the 2D Ising value, $2 - \eta = 7/4$ [34]. Inside the $\mathbf{N}$ phase, because of the circular symmetry, χ_1 gives results equivalent to the paramagnetic phase, while once in the phase $\mathbf{F}_2$ the critical nature of this phase presents an always diverging susceptibility, but with a temperature-dependent, nonuniversal exponent, and the curves do not collapse away from the transition. The bottom panel shows a good data collapse of χ_1 against the Binder cumulant [46,47], Eq. (4), with no required knowledge of the critical temperature. The scaling of the Binder cumulant, close to the transition, is $U_1 = h(L/\xi)$, where $h(x)$ is a scaling function and ξ is the correlation length. Also, since $\chi_1 = L^{2-\eta} g(L/\xi)$, we expect that $\chi_1 L^{\eta-2} = g[h^{-1}(U_1)]$. When plotted as a function of the temperature (not shown), the Binder cumulant indeed assumes (roughly) the same value for different system sizes at the transition (although, in principle, the value of U at the transition may give some information on the universality class of the transition, it seems to depend also on the boundary conditions, shape of the system and symmetry of the interactions; see Ref. [55] and references therein).

Reference [34] presented preliminary data that seemed to indicate that the transition $\mathbf{F}_1$-$\mathbf{F}_0$ was also of BKT type. However, the behavior of the helicity discussed above hints at a second-order transition. Indeed, in the region where one would expect a transition (close to the line $T_{\mathrm{KT}}(0)(1 - \Delta)$, e.g., $T \simeq 0.2$ for $\Delta = 0.8$), there is a sudden change of the helicity, but it does not scale with the system size, indicating that in the thermodynamic limit the discontinuity associated with the BKT transition is not present. Nonetheless, fractional vortices unbind at this transition, as seen by the behavior of ρ_v in the bottom panel of Fig. 3. In both $\mathbf{F}_1$ and $\mathbf{F}_0$ phases, see Fig. 5, the average distribution of orientations has a single peak that continuously becomes more narrow as the temperature decreases. Inside the phase $\mathbf{F}_0$, the variance of the distribution is larger than $\pi/8$, m_8 maps it onto the whole circle and does not distinguish it from the paramagnetic phase [see bottom panels of Fig. 5(a)]. The transition to the $\mathbf{F}_1$ phase occurs when the width becomes smaller than this value and corresponds to a strong increase of χ_8 at the transition, as shown in Fig. 7 for $\Delta = 0.8$ and 0.9. Notice that although the exponent of the susceptibility differs in both cases, for $\Delta = 0.9$ it is compatible with the Ising value. Whether this discrepancy is real and the transition line has nonuniversal, changing exponents, or whether it is caused by the proximity to the second multicritical point where all three phases $\mathbf{F}_i$ meet, is still an open question and requires further simulations. Thus, the overall evidence points to a second order transition between phases $\mathbf{F}_0$ and $\mathbf{F}_1$ compatible with the Ising universality class, at least on the rightmost part of such line.

Finally, the transition between the phases $\mathbf{F}_1$ and $\mathbf{F}_2$ is the more elusive one. Differently from the other two similar transitions, in which one specie of vortices decouples despite being second order, here both species remain bound in vortex-antivortex pairs across the transition line, Fig. 3. The helicity is not able to detect the transition as there is no difference in the cost to produce an overall twist in the system since the density of (anti)vortices, that are responsible for the stiffness, barely changes. Therefore, the best evidence we have for this transition comes from the susceptibility and the Binder cumulant. Figure 5 shows that the distribution of spin orientations is either a single peak (phase $\mathbf{F}_1$) or several peaks of different heights concentrated on a half-plane (phase $\mathbf{F}_2$). The appropriate order parameter in this transition is thus m_4, and Fig. 8 shows the corresponding fluctuations, χ_4. Notice

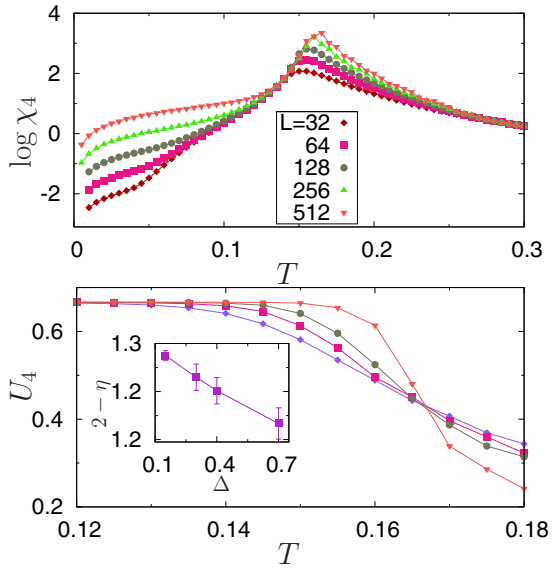

FIG. 8. (Top) Susceptibility χ_4 vs. temperature for $q = 8$ at the $\mathbf{F}_1$-$\mathbf{F}_2$ transition for $\Delta = 0.4$. (Bottom) Binder cumulant, for different sizes, crossing in the region of the putative transition. Inset: the exponent of χ_4 along the transition line showing a dependence, for the sizes considered here, on Δ.

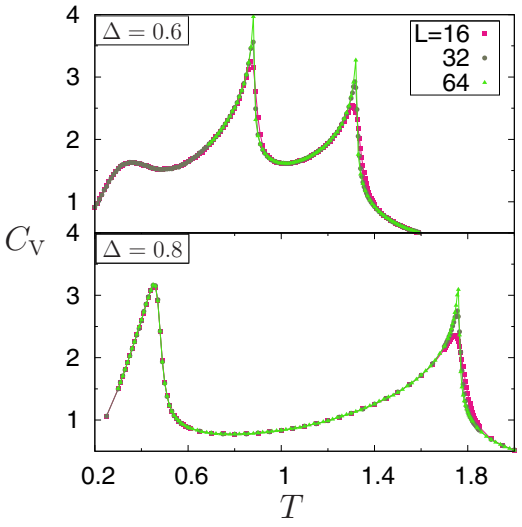

FIG. 9. Specific heat of the generalized 3D XY model for $q = 8$ and $\Delta = 0.6$ (top) and 0.8 (bottom). Although several peaks are visible, those occurring at the lowest temperature seem not to increase with the system size (see discussion in the text), while the others have the characteristic form of a λ transition, with a cusp at a finite value instead of a divergence (negative α). The overall evidence indicates that these low T peaks do not correspond to a phase transition, but to a crossover.

that the shape of these curves differs from the previous cases in which the plateau corresponding to the critical nature of a BKT phase was much higher. Here, although such a plateau seems to be developing, it is yet far from merging with the peak, what may also indicate the presence of strong finite size effects. For different system sizes, in the same region where the peak increases, we also observe, Fig. 8 (bottom), the crossing of the Binder cumulant. The inset of Fig. 8 (bottom) shows that the critical exponent $2 - \eta$ of χ_4, as measured with the available sizes, seems to depend on Δ, continuously decreasing from, roughly, 1.27 to 1.21 along the $\mathbf{F}_1$-$\mathbf{F}_2$ line. We do not rule out that larger system sizes and logarithmic corrections, when taken into account, may play a role either restoring universality or pointing to a crossover instead of a transition. Otherwise, there may exist an yet unexplored [56] connection with the Ashkin-Teller [57–60] or the eight vertex model [61–63].

B. 3D

We now address the interesting question of whether the existing ordered phases, their splitting as q increases, and the nature of the related transitions are specific to the 2D version of the model or also occur in other dimensions as well. In this section, the results obtained for $q = 3$ and 8 in 3D are presented and compared with the 2D case. Similar to the latter, the phase diagrams are sketched using the specific heat (an example, described later, is shown in Fig. 9 for $q = 8$ and two values of Δ, 0.6 and 0.8). Figure 10 shows these qualitative phase diagrams for the generalized 3D XY model with $q = 3$ (left) and 8 (right). Instead of being of BKT nature, a common feature of both cases is that the transitions between the ordered and the paramagnetic phases (**N**-**P** and $\mathbf{F}_0$-**P**) are second order and belong to the 3D XY universality class, whose critical exponents are $\beta \simeq 0.349$, $\gamma \simeq 1.318$, $\nu \simeq 0.672$, and $\alpha \simeq -0.015$ [64,65]. The exponent α of the specific heat, being negative, indicates the presence of a cusp instead of a divergence (lambda transition).

For $q = 3$, the phase diagram (Fig. 10, left) presents the same structure in both $d = 2$ and 3 [34,35]. The extreme points $\Delta = 0$ and 1 are equivalent to the original 3D XY model, with the same transition temperature. Moreover, the ground state is ferromagnetic for all values of Δ except $\Delta = 0$ where the alignment has $\pi/3$ long-range nematic order (although it may be different when antiferromagnetic interactions are considered [14]). In analogy to the 3D three states Potts model, the transition $\mathbf{F}_0$-**N** is discontinuous, as shown by the abrupt jump on the magnetization m_1 in the top panel of Fig. 11. On the other hand, the transitions to the paramagnetic phase, from both **N** and $\mathbf{F}_0$ phases, are continuous and belong to the 3D XY universality class. We show in the middle panel of Fig. 11, for $\Delta = 0.25$, that the susceptibility peak corresponding to m_3 at the transition **N**-**P** grows as $\chi_3(T_c) \sim L^{1.977(3)}$, with $T_c \simeq 1.652$, very close to the expected $\gamma/\nu \sim 1.96$ value. We also measured the helicity modulus whose behavior in the critical region is continuous [5,64,66,67] and given by $\Upsilon \sim t^{\upsilon}$, where υ is the critical exponent and t is the reduced temperature. Assuming the universal scaling function $\Upsilon(T,L) = L^{-\upsilon/\nu} g(tL^{1/\nu})$, and using the scaling law $\upsilon/\nu = d - 2 = 1$ [5,64], $L\Upsilon(T_c,L) = g(0)$ must be independent of the system size at the transition. Indeed, the bottom panel of Fig. 11 shows the rescaled helicity at the transition **N**-**P** for $\Delta = 0.25$, with all curves intersecting at $T_c \simeq 1.652$, consistent with the value obtained via susceptibility.

Figure 10 (right) shows the phase diagram for $q = 8$. Instead of the three ferromagnetic-like phases in the 2D case, only two remain in 3D (we denote the intermediate phase by

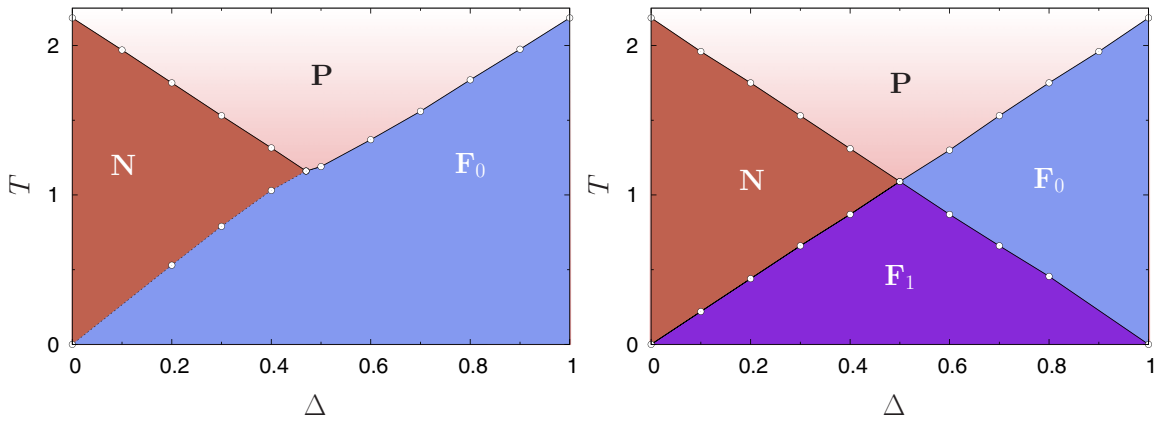

FIG. 10. Phase diagrams of the generalized 3D XY model for $q = 3$ (left) and $q = 8$ (right). The lines are just guide to the eyes and points correspond to the maximum of the specific heat for $L = 20$. In both cases, the multicritical point is close to $\Delta_{mc} \simeq 0.5$. At both $\Delta = 0$ and 1, the critical temperature is $T_c \simeq 2.202$. With the exception of the **N**-$\mathbf{F}_0$ transition for $q = 3$ that is discontinuous (dashed line), all other transitions are continuous. As discussed in the text, some uncertainty remains for the $\Delta > 0.8$ part of the $\mathbf{F}_1$-$\mathbf{F}_0$ line.

$\mathbf{F}_1$). As mentioned before, the transition to the paramagnetic phase, from both **N** and $\mathbf{F}_0$, are in the 3D XY universality class. We now discuss the properties of the transitions involving the intermediate phase, $\mathbf{F}_1$-**N** and $\mathbf{F}_1$-$\mathbf{F}_0$, and the evidences for a crossover inside the phase $\mathbf{F}_1$.

Figure 12 (top) shows the behavior of the susceptibility χ_1 for $\Delta = 0.35$ around the $\mathbf{F}_1$-**N** transition. An excellent data collapse is obtained with the critical exponents $\gamma \simeq 1.33(5)$, $\nu \simeq 0.67(1)$, and $T_c \simeq 0.771$, values that are very close to those of the 3D XY universality class. Moreover, the Binder cumulant, evaluated for different system sizes, has the typical crossing point and the rescaled data also collapses very well onto a universal curve using the same T_c and ν above, as shown in Fig. 12 (bottom). This is remarkable since in principle one would expect a symmetry breaking, 3D Ising universality class transition. Indeed, the angle distribution in these two phases is similar in both two and three dimensions (see, e.g., Fig. 5), passing from equally distributed peaks around the circle (nematic-like) to a few peaks on a single half-plane (ferromagnetic-like). Moreover, the helicity does not present the typical signature of the 3D XY transition, continuously transitioning to the value characterizing the new phase, with an intermediate, size-dependent behavior. The specific heat is of no help to decide between those universality classes, a good collapse is obtained with the above ν (closer to 3D XY) and a small but positive α (closer to 3D Ising). Therefore, our present data only partially confirm that the transition is in the 3D Ising universality class, while larger sizes and corrections

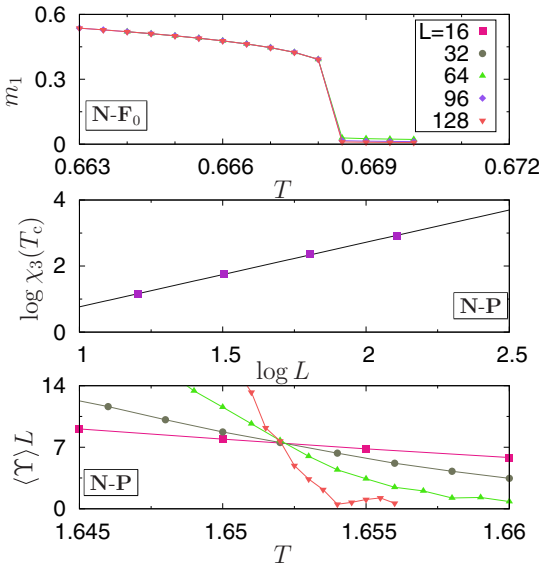

FIG. 11. Results for the $q = 3$ 3D XY model with $\Delta = 0.25$. Discontinuous magnetization vs. temperature around the transition $\mathbf{F}_0$-**N** (top panel). At the transition **N**-**P**, the peak of the susceptibility χ_3 grows as $L^{1.977(3)}$ (middle panel), while all curves for the helicity modulus intersect close to the critical temperature (bottom panel).

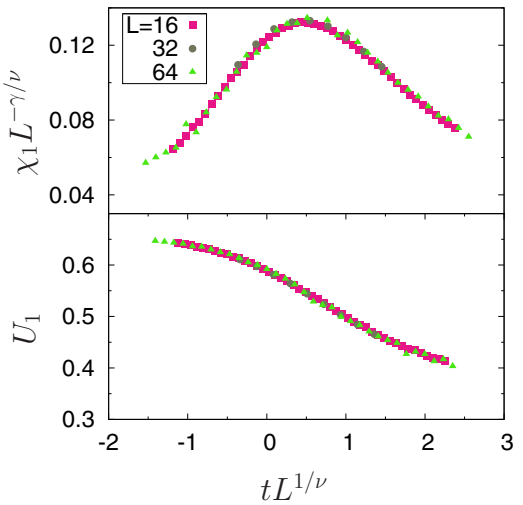

FIG. 12. Collapses of the susceptibility (top) and Binder cumulant (bottom) at the $\mathbf{F}_1$-**N** transition for $q = 8$ and $\Delta = 0.35$ with $T_c = 0.771$ and the exponents $\gamma \simeq 1.33(5)$ and $\nu \simeq 0.67(1)$, whose values are close to those of the 3D XY model.

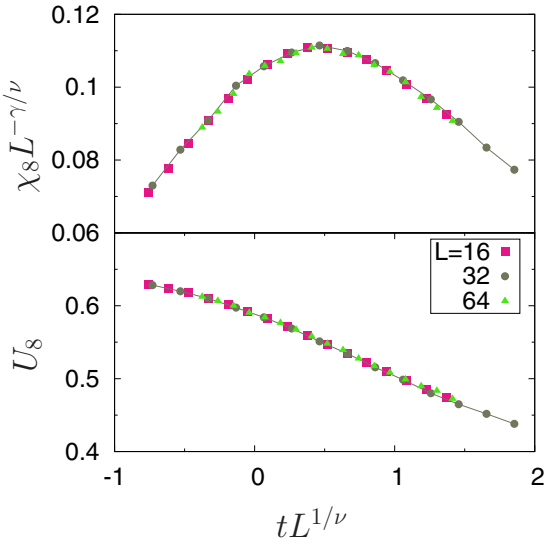

FIG. 13. $\mathbf{F}_1$-$\mathbf{F}_0$ transition for $q = 8$ and $\Delta = 0.6$ in 3D. (Top) Susceptibility vs. temperature for the 3D collapses onto a universal curve with $T_c = 0.881$ and exponents $\gamma \simeq 1.33(1)$, $\nu \simeq 0.67(1)$. (Bottom) Collapse of the Binder cumulant using the same values.

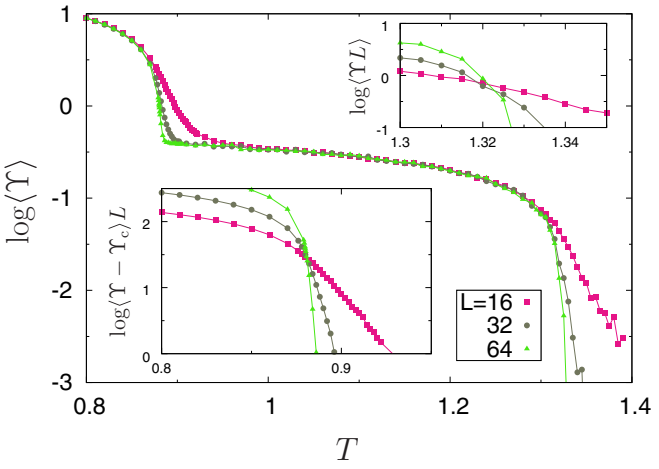

FIG. 14. Helicity modulus versus temperature in 3D for $q = 8$, $\Delta = 0.6$, and several system sizes. The two transitions can be seen as two jumps, first to a finite value ($\Upsilon_c \simeq 0.404$) at the $\mathbf{F}_1$-$\mathbf{F}_0$ transition ($T_c \simeq 0.88$) and then to zero at the $\mathbf{F}_0$-$\mathbf{P}$ transition ($T_c \simeq 1.32$). At both transitions, the helicity, conveniently rescaled, crosses at the critical temperature for different values of L, as shown in the two insets, bottom and top, respectively.

to the scaling will be necessary to obtain a better estimate of the exponents.

The transition $\mathbf{F}_1$-$\mathbf{F}_0$ also seems to be in the 3D XY universality class (but see below). Indeed, Fig. 13 (top) shows the collapsed susceptibility χ_8 around $T_c \simeq 0.88$, for $\Delta = 0.6$, with the critical exponents $\gamma \simeq 1.33(1)$ and $\nu \simeq 0.67(1)$, once again close to those of the 3D XY universality class. At this critical temperature, the Binder cumulant also presents a crossing point for several system sizes and in the bottom part of Fig. 13 its collapse using the same exponent ν and T_c is shown. Figure 14 shows the helicity modulus for the same Δ. Inside each phase it has a size-independent value, with all curves collapsing onto each other, as in 2D. At the two transitions ($\mathbf{F}_1$-$\mathbf{F}_0$ and $\mathbf{F}_0$-$\mathbf{P}$ at $T_c \simeq 0.88$ and 1.32, respectively) there is a continuous change of Υ toward the value at the transition ($\Upsilon_c \simeq 0.404$ and 0, respectively). From the previous discussion of Υ, we expect a power law behavior at the transition, $\Upsilon - \Upsilon_c \sim t^{\upsilon}$, with $\upsilon = \nu$. A good collapse (not shown) is obtained with values very close to the T_c and $\nu = \upsilon$ obtained from the susceptibility. Moreover, the specific heat for this case is shown in the top panel of Fig. 9. The first peak on the left is believed to correspond to a crossover (see below) while the rightmost one is associated to the transition to the paramagnetic state. The behavior of the intermediate specific heat peak, instead, is consistent with a lambda transition and, indeed, $\alpha < 0$ for the 3D XY universality class.

The results are less clear at the far right region of the phase diagram and how and whether the $\mathbf{F}_1$-$\mathbf{F}_0$ transition line extends beyond this point is still an open problem. For example, for $\Delta = 0.8$ (similar results were obtained for $\Delta = 0.9$ as well), the specific heat in Fig. 9 (bottom) has only two peaks, one that clearly corresponds to the λ transition at higher temperatures while the other one, at lower temperature, does not present any size dependence on the range of system sizes considered here. The same behavior is observed in the helicity, Fig. 15: although two sudden decreases are observed as the temperature increases, only the one at the highest T presents a size dependence compatible with a continuous transition (inset). The other one, corresponding to the first peak of the specific heat, does not change with the system size. Notice that, as discussed below, there is a crossover line inside phase $\mathbf{F}_1$ that meets the $\mathbf{F}_1$-$\mathbf{F}_0$ close to $\Delta = 0.8$, what may perhaps explain the odd behavior in this case.

Finally, we investigate the possible existence of a phase $\mathbf{F}_2$ similar to the 2D case. Small systems behave as if another transition indeed exists inside the $\mathbf{F}_1$ phase: both the specific heat (Fig. 9 for $\Delta = 0.6$) and the susceptibility χ_4 (Fig. 16 for $\Delta = 0.4$) present a peak in that region. However, by increasing

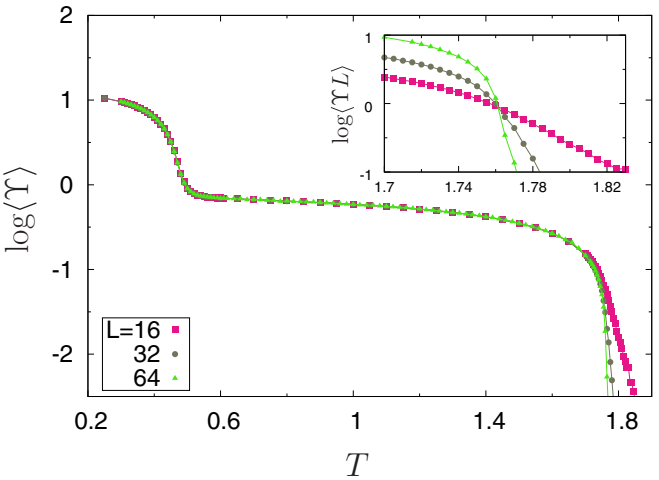

FIG. 15. The same as in Fig. 14 but with $\Delta = 0.8$. Notice that although the helicity has a sudden decrease around $T \simeq 0.4$, it does not present any size dependence.

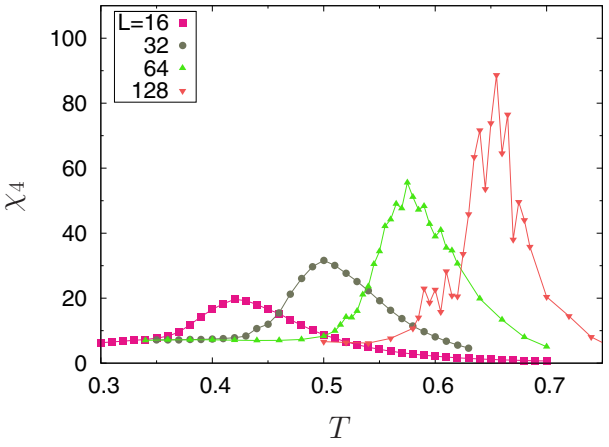

FIG. 16. Susceptibility χ_4 vs. temperature for $\Delta = 0.4$ and $q = 8$ in 3D showing that, for small system sizes, it develops a peak at a temperature below the $\mathbf{F}_1$-$\mathbf{F}_0$ transition (that, in 2D, corresponds to the actual transition $\mathbf{F}_1$-$\mathbf{F}_2$). However, as L increases, this peak moves to the right, toward the $\mathbf{F}_2$-$\mathbf{N}$ boundary at $T_c \simeq 0.88$.

the system size, all the evidence points to a crossover instead of a genuine transition. While the specific heat peak of Fig. 9 (top) does not change in height, the susceptibility in Fig. 16 does increase in size while, at the same time, moving to higher temperatures. With our present data, it seems that this line moves toward the boundary with the **N** phase, a pure crossover.

III. CONCLUSIONS

We performed extensive simulations for a generalization of the continuous spin XY model that introduces competition between different local alignments. Despite both terms in the Hamiltonian, Eq. (1), having the same symmetry under uniform rotations, each one induces a different local ordering: while the ferromagnetic term tends to align the spins, the nematic one tries to have them either parallel or dephased by the multiples of $2\pi/q$ (a nematic configuration). While the former configuration is favored by both terms, the latter has some degree of frustration and only appears at higher temperatures, whatever the value of $q > 1$. The low-temperature phase, on the other hand, has a local ferromagnetic ordering that, in both 2 and 3 dimensions, unfolds through a sequence of phase splittings, as q increases, into several phases with similar ferromagnetic ordering. As a consequence, for $q \geqslant 4$ this model has intermediate phases ($0 < \Delta < 1$) driven by the competition of both terms in Eq. (1), except for $\Delta = 0$ and 1 where a single phase exists, with either local nematic or ferromagnetic alignment, respectively. It is interesting that the appearance of a new phase below the nematic one, and the subsequent splitting and growth is very similar to the sequence appearing in the discrete, $\mathbb{Z}_q$ symmetry Clock model. Indeed, in 2D the transition to phase **N** is in the Ising ($q = 2$ and 4) or 3 states Potts model ($q = 3$) universality class. All phases below the paramagnetic transition are critical in the BKT sense (e.g., power-law decaying correlations and divergent susceptibility, with nonuniversal exponents, at all temperatures). Associated with that, the model presents multiple transitions as the temperature changes, some with the BKT signature, while others are discrete symmetry breaking transitions embedded into these critical regions. These phases may contain integer and/or fractional vortices, which can be bound or unbound. While for $q = 2$ and 3 the low temperature phase is dominated by the integer vortices of phase $\mathbf{F}_0$, for $q = 8$ (and probably for any $q > 3$), these integer vortices coexist, in the competition induced phases, with fractional vortices and topological defects at sufficiently low temperatures. Remarkably, having vortices decoupling at a transition is not a sufficient condition for this transition to be of BKT type. Indeed, as an example, entering the $\mathbf{F}_0$ phase (whose bound vortices are integer) from $\mathbf{F}_1$ or $\mathbf{F}_2$ (both populated with two species of bound vortices) may be either a BKT or an Ising transition, respectively. Moreover, for a second-order transition, decoupling is not even necessary as it does not occur at the $\mathbf{F}_1$-$\mathbf{F}_2$ transition. We may also view the interplay between the two terms in Eq. (1) as a way to choose which species of vortices to suppress or enhance [54,68] by tuning Δ and T.

A BKT transition is signaled by a discontinuity in the helicity modulus that, for a finite system, appears as a size dependence on the intersection of Υ with a given reference line. When there was a sudden, significant change in the helicity, but finite-size effects were absent, we assumed it to be an indication that the transition is second order (another possibility, one that occurs in the 3D case, is a crossover). However, the true nature of some of the transitions reported here is only observed for systems too large to be simulated on a single CPU. It was only through the power made available by GPU processing that we were able to obtain our results, and even so, this characterization is not always very clear, with a few regions, both in two and three dimensions, that deserve further studies. In the case of the $\mathbf{F}_1$-$\mathbf{F}_2$ transition occurring for $q = 8$ in 2D, not even this extra computational aid was sufficient. Further work is therefore necessary in order to make sure that the transition is real and if so, obtain more precise estimates for the critical exponents, deciding whether they depend or not on Δ, as the results so far indicate. In the 3D case, although there seems to exist a single intermediate phase as the 2D $\mathbf{F}_1$-$\mathbf{F}_2$ transition turns into a crossover, there is some uncertainty regarding the extension of the $\mathbf{F}_1$-$\mathbf{F}_0$ line beyond $\Delta \simeq 0.8$ as several quantities behave qualitatively different from the $\Delta = 0.6$ case (compare, e.g., the first shoulder in Figs. 14 and 15). It would take larger systems and longer simulation times in order to properly access these issues, which is beyond our current computational capabilities.

Recently, a new universality class has been studied [69] in models where the BKT transition meets a $\mathbb{Z}_2$ (Ising) transition line at a multicritical point. This point seems to have properties of supersymmetry. We conjecture that this may also be the case for the multicritical point exibited by the generalized XY model in 2D with $q = 2$, that presents both U(1) and $\mathbb{Z}_2$ symmetry properties. It is thus of interest to study not only the properties of the multicritical point in this model, but also to see whether it conforms with the predictions of Ref. [69] and whether this applies as well for $q = 3$ where the line is in the Potts universality class or for larger values of q. Moreover, for $q > 4$ there is a second multicritical point that is at the triple border between the three $\mathbf{F}_i$ phases. The behavior at this point and whether it is similar to the other

one is an yet open problem. It would be interesting to study the properties of these multicritical points in order to check whether the behavior of the correlation length differs both from a conventional second order transition and from a BKT one as predicted in Ref. [69]. Further possible extensions include noninteger values of q, antiferromagnetic interactions [70], or a generalized version with discrete spins (studied for $q = 2$ in Ref. [71]). Trying to disentangle the roles of the two terms in the Hamiltonian, by introducing two variables per site and an onsite coupling between them [17,32,38,40,41], may also be helpful to better understand the new phases for $q > 4$. These questions, together with a better description of the geometry of topological defects are left for a future work.

ACKNOWLEDGMENTS

Research partially supported by the Brazilian agencies CNPq, CAPES, and Fapergs. J.J.A. acknowledges the INCT-Sistemas Complexos (CNPq) for partial support and interesting discussions with M. Picco and F. Corberi. Y.L. acknowledges partial support of INCT-FCx and of US-AFOSR under Grant No. FA9550-16-1-0280.

[1] N. D. Mermin and H. Wagner, Phys. Rev. Lett. **17**, 1133 (1966).
[2] V. L. Berezinskii, Sov. Phys. JETP **32**, 493 (1971).
[3] J. M. Kosterlitz, J. Phys. C: Solid State Phys. **7**, 1046 (1974).
[4] J. M. Kosterlitz and D. J. Thouless, J. Phys. C: Solid State Phys. **6**, 1181 (1973).
[5] M. E. Fisher, M. N. Barber, and D. Jasnow, Phys. Rev. A **8**, 1111 (1973).
[6] D. R. Nelson and J. M. Kosterlitz, Phys. Rev. Lett. **39**, 1201 (1977).
[7] T. Ohta and D. Jasnow, Phys. Rev. B **20**, 139 (1979).
[8] M. Hasenbusch, J. Phys. A: Math. Gen. **38**, 5869 (2005).
[9] Y. Shi, A. Lamacraft, and P. Fendley, Phys. Rev. Lett. **107**, 240601 (2011).
[10] D. M. Hübscher and S. Wessel, Phys. Rev. E **87**, 062112 (2013).
[11] D. Malkar, B. Sadashiva, and A. Roy, Soft Matter **12**, 4960 (2016).
[12] G. M. Grason, Europhys. Lett. **83**, 58003 (2008).
[13] A. B. Cairns, M. J. Cliffe, J. A. M. Paddison, D. Daisenberger, M. G. Tucker, F.-X. Coudert, and A. L. Goodwin, Nat. Chem. **8**, 442 (2016).
[14] M. Žukovič, Phys. Rev. B **94**, 014438 (2016).
[15] L. Bonnes and S. Wessel, Phys. Rev. B **85**, 094513 (2012).
[16] M. J. Bhaseen, S. Ejima, F. H. L. Essler, H. Fehske, M. Hohenadler, and B. D. Simons, Phys. Rev. A **85**, 033636 (2012).
[17] L. de Forges de Parny, A. Rançon, and T. Roscilde, Phys. Rev. A **93**, 023639 (2016).
[18] S. Ngo, F. Ginelli, and H. Chaté, Phys. Rev. E **86**, 050101(R) (2012).
[19] T. J. Krieger and H. M. James, J. Chem. Phys. **22**, 796 (1954).
[20] S. E. Korshunov, JETP **41**, 263 (1985).
[21] S. E. Korshunov, J. Phys. C: Solid State Phys. **19**, 4427 (1986).
[22] D. H. Lee and G. Grinstein, Phys. Rev. Lett. **55**, 541 (1985).
[23] D. H. Lee, G. Grinstein, and J. Toner, Phys. Rev. Lett. **56**, 2318 (1986).
[24] D. B. Carpenter and J. T. Chalker, J. Phys.: Condens. Matter **1**, 4907 (1989).
[25] P. I. C. Teixeira, Liq. Cryst. **25**, 721 (1998).
[26] M. Dian and R. Hlubina, Phys. Rev. B **84**, 224420 (2011).
[27] J.-P. Lü and Q.-H. Chen, Commun. Theor. Phys. **57**, 166 (2012).
[28] D. Johnson, D. Allender, R. de Hoff, C. Maze, E. Oppenheim, and R. Reynolds, Phys. Rev. B **16**, 470 (1977).
[29] R. M. Hornreich and S. Shtrikman, Phys. Lett. A **63**, 39 (1977).
[30] D. J. Amit, S. Elitzur, E. Rabinovici, and R. Savit, Nucl. Phys. B **210**, 69 (1982).
[31] F. C. Alcaraz, L. Jacobs, and R. Savit, Nucl. Phys. B **265**, 161 (1986).
[32] E. Granato, J. M. Kosterlitz, and J. Poulter, Phys. Rev. B **33**, 4767 (1986).
[33] F. Shahbazi and R. Ghanbari, Phys. Rev. E **74**, 021705 (2006).
[34] F. C. Poderoso, J. J. Arenzon, and Y. Levin, Phys. Rev. Lett. **106**, 067202 (2011).
[35] G. A. Canova, Y. Levin, and J. J. Arenzon, Phys. Rev. E **89**, 012126 (2014).
[36] J. E. Van Himbergen, Phys. Rev. B **34**, 6567 (1986).
[37] S. Romano, Phys. Rev. E **73**, 042701 (2006).
[38] R. Bruinsma and G. Aeppli, Phys. Rev. Lett. **48**, 1625 (1982).
[39] I. M. Jiang, S. N. Huang, J. Y. Ko, T. Stoebe, A. J. Jin, and C. C. Huang, Phys. Rev. E **48**, R3240 (1993).
[40] R. Ghanbari and F. Shahbazi, Phys. Rev. E **72**, 021709 (2005).
[41] C.-C. Shih and I.-M. Jiang, Physica A **358**, 366 (2005).
[42] U. Wolff, Phys. Rev. Lett. **62**, 361 (1989).
[43] R. H. Swendsen and J.-S. Wang, Phys. Rev. Lett. **58**, 86 (1987).
[44] O. Kalentev, A. Rai, S. Kemnitz, and R. Schneider, J. Parallel Distrib. Comput. **71**, 615 (2011).
[45] L. Y. Barash and L. N. Shchur, Comput. Phys. Commun. **185**, 1343 (2014).
[46] D. Loison, J. Phys.: Condens. Matter **11**, L401 (1999).
[47] M. Hasenbusch, J. Stat. Mech. (2008) P08003.
[48] P. Minnhagen and B. J. Kim, Phys. Rev. B **67**, 172509 (2003).
[49] J. Tobochnik and G. V. Chester, Phys. Rev. B **20**, 3761 (1979).
[50] C. M. Lapilli, P. Pfeifer, and C. Wexler, Phys. Rev. Lett. **96**, 140603 (2006).
[51] J. V. José, L. P. Kadanoff, S. Kirkpatrick, and D. R. Nelson, Phys. Rev. B **16**, 1217 (1977).
[52] Y. Kumano, K. Hukushima, Y. Tomita, and M. Oshikawa, Phys. Rev. B **88**, 104427 (2013).
[53] H. Weber and P. Minnhagen, Phys. Rev. B **37**, 5986 (1988).
[54] H. J. Jensen and H. Weber, Phys. Rev. B **45**, 10468 (1992).
[55] A. Malakis, N. G. Fytas, and G. Gülpinar, Phys. Rev. E **89**, 042103 (2014).
[56] V. Aji and C. M. Varma, Phys. Rev. B **79**, 184501 (2009).
[57] J. Ashkin and E. Teller, Phys. Rev. **64**, 178 (1943).
[58] G. S. Grest and M. Widom, Phys. Rev. B **24**, 6508 (1981).
[59] R. Badke, P. Reinicke, and V. Rittenberg, J. Phys. A: Math. Gen. **18**, 73 (1985).
[60] Y. Y. Goldschmidt, Phys. Rev. Lett. **56**, 1627 (1986).

[61] B. Sutherland, J. Math. Phys. **11**, 3183 (1970).
[62] R. Baxter, Phys. Rev. Lett. **26**, 832 (1971).
[63] L. P. Kadanoff and F. J. Wagner, Phys. Rev. B **4**, 3989 (1971).
[64] Y.-H. Li and S. Teitel, Phys. Rev. B **40**, 9122 (1989).
[65] M. Campostrini, M. Hasenbusch, A. Pelissetto, and E. Vicari, Phys. Rev. B **74**, 144506 (2006).
[66] A. P. Gottlob and M. Hasenbusch, Physica A **201**, 593 (1993).
[67] I.-H. Jeon, J.-G. Shin, and M.-C. Cha, J. Korean Phys. Soc. **60**, 581 (2012).
[68] S. Bhattacharya and P. Ray, Phys. Rev. Lett. **116**, 097206 (2016).
[69] L. Huijse, B. Bauer, and E. Berg, Phys. Rev. Lett. **114**, 090404 (2015).
[70] M. Žukovič and T. Idogaki, Physica B **328**, 377 (2003).
[71] C. Chatelain, J. Stat. Mech. (2016) P073306.